Available online at www.sciencedirect.com
ScienceDirect
Agricultural and Forest Meteorology 145 (2007) 149–166
AGRICULTURAL AND FOREST METEOROLOGY
www.elsevier.com/locate/agrformet

Cold air drainage in a forested valley: Investigating the feasibility of monitoring ecosystem metabolism

T.G. Pypker [a,e,*], M.H. Unsworth [a], B. Lamb [b], E. Allwine [b], S. Edburg [b], E. Sulzman [c], A.C. Mix [a], B.J. Bond [d]

[a] College of Oceanic and Atmospheric Sciences, Oregon State University, Corvallis, OR 97331, USA
[b] Department of Civil Engineering, Washington State University, WA 99164, USA
[c] Department of Crop and Soil Science, Oregon State University, Corvallis, OR 97331-5752, USA
[d] Department of Forest Science, Oregon State University, Corvallis, OR 97331-5752, USA
[e] School of Forest Resources and Environmental Science, Michigan Technological University, Houghton, MI 49931-1295, USA

Received 24 August 2006; received in revised form 6 February 2007; accepted 19 April 2007

Abstract

Our objectives were to: characterize spatial and temporal variation in wind speed, direction and air temperature within a steeply sloping 96 ha forested watershed in the Oregon Cascade Mountains; assess the area contributing to advection in cold air drainage; identify appropriate conditions for sampling advected gases representative of the entire watershed; estimate ecosystem respiration from mass balance estimates. The flow dynamics could be categorized into four periods: daytime flows, evening transition, nighttime conditions (formation of a cold air pool) and morning transition. On summer days, the wind above the canopy flowed up-valley whereas the wind direction below the canopy was often down-valley. During the evening transition, the below-canopy cold air drainage became well mixed after the vertical temperature profile at the tower became isothermal, and sodar and tethersonde data revealed that a second drainage flow developed above the canopy. Between 20:00 and 24:00 h (PST), a cold air pool formed within the valley; cold air drainage continued, but wind speed decreased as the night progressed. After sunrise, CO_2 in air passing the tower remained well mixed, but its concentration decreased. After the base of the watershed began to receive direct solar radiation, the in-canopy vertical CO_2 concentration profile became stratified and the cold air drainage ceased or was confined below the canopy.

After the cold air pool formed, the entire watershed supplied the respired CO_2 that advected past the tower. During this period, the potential temperature profile within the watershed indicated a strong inversion within the watershed. Because the air passing the tower was well mixed and the cold air pool encompassed the entire watershed, it is probable that air samples collected during this period could provide the best estimate of watershed-scale respiration and carbon isotope composition of respired CO_2 (Keeling plot analysis). However, sampling prior to the formation of the cold air pool may confound interpretations as the area contributing to the tower is likely changing. Mass balance calculations using an inert tracer (SF_6) released below the canopy demonstrated that data from a single vertical profile could provide plausible estimates of ecosystem respiration at the watershed scale.

Keywords: Cold air drainage; CO_2 fluxes; SF_6; Douglas-fir

1. Introduction

New tools are needed to observe how weather, climate and land-use change affect CO_2 fluxes and ecosystem metabolism in complex topography (Bowling et al., 2005; Schimel et al., 2002), as current methods are

* Corresponding author. Present address: School of Forest Resources and Environmental Science, Michigan Technological University, Houghton, MI 49931-1295, USA. Tel.: +1 906 487 1089; fax: +1 906 487 2915.
E-mail address: tgpypker@mtu.edu (T.G. Pypker).

0168-1923/$ – see front matter © 2007 Elsevier B.V. All rights reserved.
doi:10.1016/j.agrformet.2007.04.016

limited to flat terrain where micrometeorological techniques such as eddy covariance are applicable. In the mountainous regions of the Pacific Northwest, flux estimates are particularly important because these carbon rich forests (Harmon et al., 2004) are sensitive to changes in water availability (Anthoni et al., 2002; Paw et al., 2004) as well as temperature. Future climate scenarios predict that the Pacific Northwest will have higher temperatures (~2–3 °C higher by 2050) and decreased water availability (Parsons et al., 2001).

When using eddy covariance to quantify the carbon exchange of a forest, the nighttime advection of CO_2 in cold air drainages increases uncertainty in the estimates (e.g. Aubinet et al., 2003; Black et al., 1996; Lavigne et al., 1997; Paw et al., 2004; Staebler and Fitzjarrald, 2004). Cold air drainage can occur on slopes with less than 1% gradient (Mahrt, 1981; Soler et al., 2002; Stull, 1988), but the advection of momentum, mass and energy is much greater in areas with steeper slopes. There have recently been some important steps in quantifying the effect of advection on estimates of CO_2 fluxes at eddy covariance sites that are located in areas with modestly sloping terrain (Staebler and Fitzjarrald, 2004; Yi et al., 2005). For example, Yi et al. (2005) successfully modeled the advection of CO_2 at their research site at Niwot Ridge, CO. However, although Niwot Ridge is located in relatively complex terrain, the slope of the land (5–6°) is shallow compared to many of the slopes found in the mountainous Pacific Northwest. Thus, while such research has provided insight into methods for quantifying advection, it does not provide a micrometeorological tool for monitoring carbon fluxes in mountainous terrain.

Mountain ecosystems differ from flat land in their ecosystem–atmosphere carbon exchange because of spatial variability in radiation interception, soil properties and water availability associated with steeply sloping terrain. Although steep slopes are unsuitable for most micrometeorological flux measurement methods, they offer the potential for observing watershed-scale advected fluxes of scalars in the katabatic air drainage flows that develop on slopes on otherwise still, clear nights (Pypker et al., 2007). To interpret observed concentrations of CO_2 in drainage flow we require improved understanding of the dynamics of the cold air drainage in forested watersheds and of how CO_2 monitored in the drainage flow is influenced by ecosystem metabolism.

In mountain valleys, disproportionate heating and cooling results in different air densities at the same altitude, thereby creating up-valley (anabatic) flow during the day and down-valley (katabatic) flow at night (termed cold air drainage in this paper) (Doran et al., 1990; Fleagle, 1950; Mahrt and Larsen, 1982; Manins and Sawford, 1979; Whiteman, 1990). As the cold air drains down-valley at night it gains CO_2 respired from below- and above-ground ecosystem components. Past work at the H.J. Andrews Experimental Forest (Central Oregon Cascade Mountains) has demonstrated that isotopic composition of respired CO_2 and approximate fluxes of CO_2 can be quantified by monitoring the air at various heights on a tower located at the base of a deeply incised watershed (20–33° slope) (Pypker et al., 2007). However, to utilize the information contained within the cold air drainage flow to interpret ecosystem processes one must first gain a better understanding of the drainage dynamics.

Past research on the watershed monitored in this study (Pypker et al., 2007) revealed that cold air drainage occurred on more than 80% of summer nights, was greater than 28 m deep near the bottom of the valley, and had the typical S-shaped wind speed profile in the canopy as reported by others (e.g. Allen, 1968; Fons, 1940; Landsberg, 1971; Shaw, 1977; Turnipseed et al., 2003). Wind speeds were maximum near the ground and minimum within the region of greatest foliage density. Preliminary analysis also indicated that the additional CO_2 (above the background concentration) advected in the bottom 28 m of the cold air drainage flow at the base of the valley appeared to be only a small fraction of the likely CO_2 respired within the watershed.

The range of CO_2 concentrations observed during a single night was sufficient to determine the isotopic composition of respired CO_2 using 'Keeling plot analysis' (Keeling, 1958, 1961). However, questions remained regarding the structure of the flow, the area of the watershed contributing to the advected flux of CO_2 at the tower (the 'footprint'), and the exchange of CO_2 between the cold air drainage and the overlying air. Without this information, it is difficult to determine the appropriate time for collecting representative air samples for isotope analysis and to estimate the flux of CO_2 respired by the ecosystem, and it is difficult to interpret results in an ecosystem context.

The overall goal of this study is to facilitate the monitoring of ecosystem metabolism in complex terrain, as revealed by nocturnal respiration rates and isotopic composition of respired CO_2, by making measurements in cold air drainage. To extend our understanding of the development and structure of cold air drainage at the research site beyond that reported in Pypker et al. (2007), we installed additional sonic anemometers, temperature sensors and CO_2 profiling systems on a tower placed near the bottom of the

watershed. We also released an inert gaseous tracer (SF_6) in the watershed, monitoring its concentration at the tower and up the valley slopes, and we measured wind speed, direction and air temperature above the forest canopy using a sodar and a tethersonde. The objectives of this paper are to: (1) characterize the wind and temperature variation in time and space within the watershed; (2) identify appropriate conditions for sampling advected gases representative of the entire watershed; (3) estimate components of the mass budgets of SF_6 and CO_2 in the watershed.

2. Materials and methods

2.1. Study site

The study area was a steep V-shaped watershed that has been used for many years for studies of hydrology, ecology and physiology in the H.J. Andrews Experimental Forest located within the western Cascades of central Oregon, USA (44.2°N, 122.2°W). The watershed (Watershed 1) is part of a Long-Term Ecological Research (LTER) site supported by the National Science Foundation. The watershed is mostly covered by young Douglas-fir (*Psuedostuga menziesii* (Mirb.) Franco) that regenerated following clear-cut harvest in the late 1960s. A smaller component of the tree basal area is comprised of western hemlock (*Tsuga heterophylla*), big leaf maple (*Acer macrophyllum*), vine maple (*Acer circinatum*) and red alder (*Alnus rubra*), with the angiosperm populations being greatest within the riparian area adjacent to a small stream running down the axis of the valley (Moore et al., 2004). At the time of this study, the canopy was between 25 and 28 m tall and had a leaf area index ranging between 4 and 10 (data not shown). The site has wet mild winters and warm dry summers with a mean annual precipitation of 2300 mm. The warm dry summers of this region are associated with relatively cloud-free, low wind-speed conditions that allow cold air drainage to develop on most nights (Pypker et al., 2007). The soil is a gravelly clay loam (Swanson and James, 1975).

2.2. Meteorological observations

2.2.1. Tower observations

A tower located at the base of the watershed, was extended from 28 to 37 m in the Fall of 2004 (Base tower; Fig. 1a). It was instrumented in May 2005 with ten shielded thermistors (Model 107 temperature probe, Campbell-Scientific Inc., Logan, UT), a net radiometer (Q7 REBS, Campbell-Scientific Inc.), a temperature/RH

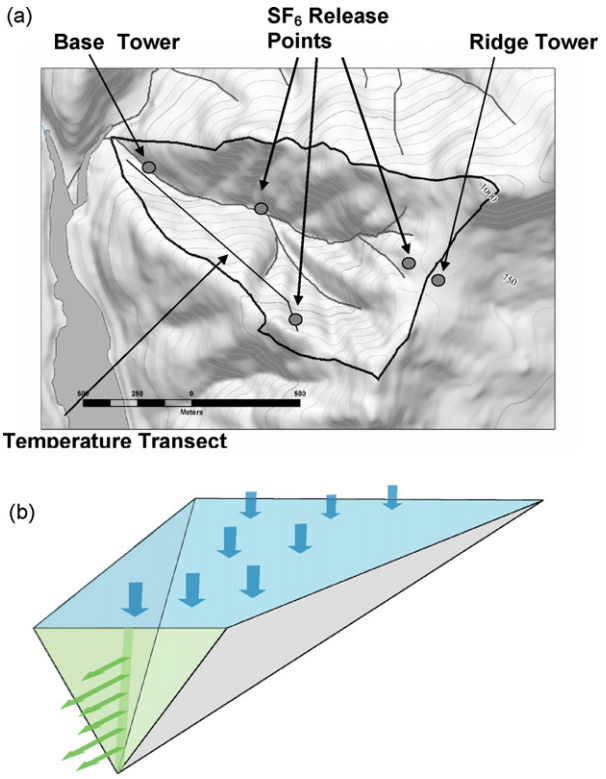

Fig. 1. (a) Map of the watershed with the locations of the 37 m base tower, temperature transect, SF_6 release point and ridgetop tower. (b) A simplified version of the watershed as used in flux estimations. In this image, the bottom of the watershed is rotated from toward the viewer to demonstrate the outflow of air at the base of the watershed.

probe (HMP45c, Campbell-Scientific Inc.), eight 2-D sonic anemometers (WS425, Vaisala, Helsinki, Finland) and two 3-D sonic anemometers (81,000, RM Young, Traverse City, MI) (Table 1). For most periods the 2- and 3-D sonic anemometers were recorded at 0.1 and 1 Hz, respectively, and values were averaged over 1 min intervals. During select periods of CO_2 or SF_6 monitoring, the 3-D sonic anemometers were recorded at 10 Hz. The remaining instruments were recorded every 1 s and averaged over 15 min intervals (using CR10X and CR23X data loggers, Campbell-Scientific Inc.).

A second tower, 19.8 m tall with a 3.7 m telescoping pole at the top, was constructed near the ridge of the watershed (Ridge tower; Fig. 1a). It was instrumented in May 2005 with a cup anemometer and wind vane at 23.5 m (05103-L RM Young Wind Monitor, Campbell Scientific Inc.), a temperature/RH probe at 19.8 m (HMP45c, Campbell-Scientific Inc.) and a thermistor at 3 m (Model 107 temperature probe, Campbell-Scientific Inc.). The instruments were recorded by a datalogger (CR10X, Campbell-Scientific Inc.) every 1 s and averaged over 15 min intervals.

Table 1
Location of instruments on a 37 m tower constructed at the base of a young Douglas-fir watershed in central Oregon

Height (m)	Instruments
37	Thermistor 2-D sonic anemometer Quantum sensor
33	Thermistor 2-D sonic anemometer
30	Thermistor 3-D sonic anemometer Net radiometer
25	Thermistor 2-D sonic anemometer
20	Thermistor 2-D sonic anemometer
15	Temperature\RH Probe 2-D sonic anemometer
10	Thermistor 3-D sonic anemometer
7	Thermistor 2-D sonic anemometer
5	Thermistor
3	Thermistor 2-D sonic anemometer
1.5	Thermistor 2-D sonic anemometer

2.2.2. Temperature transect

The spatial variability in air temperature within the watershed was measured using 30 thermistors located on a transect that stretched along the (east–west) axis of the watershed (Fig. 1a). Each of the 30 thermistors (HOBO-Pro model #H8-031-08, Onset, Bourne, MA) was installed in a radiation shield (part# RS1, Onset) 0.5 m from the ground (Fig. 1a), and recorded the air temperature once every 15 min on its individual datalogger.

2.2.3. Tethersonde and sodar measurements above the canopy

During an intensive sampling period in August 2006, the vertical profile of air temperature above the canopy top was measured using a tethersonde balloon carrying a sensor consisting of a copper–constantan thermocouple (TC6-T, Onset) and a pressure transducer (S-BPA-CM10, Onset) monitored at 1 Hz by a small datalogger (H12, Onset). The tethersonde was raised and lowered through a small clearing approximately 100 m from the tower (Fig. 1a).

The vertical profile of wind speed and direction was monitored simultaneously using a sodar (Scintec, MFAS) co-located at the tethersonde site. The sodar provided averaged 15 min wind speed and direction up to 105 m; data were stored on a laptop computer.

2.3. Carbon dioxide concentration profiles

The variation of CO_2 concentration with height was monitored 1 day per week at the base tower using a profiling system controlled by a data logger (CR21x, Campbell-Scientific Inc.). Concentrations of CO_2 were measured every second at one of five heights (3, 10, 20, 30 and 37 m) using an infra-red gas analyzer (IRGA) (Li-6262, Li-Cor Inc., Lincoln, NE, USA). The concentrations were monitored at each height for 1 min, with the average CO_2 concentration for the last 30 s being recorded by the data logger. Inlets at the remaining heights that were not being monitored by the IRGA were purged continuously by a second pump.

2.4. Release and monitoring of sulfur hexafluoride (SF_6)

Tracer experiments using SF_6 were conducted 12–14 September 2005 and 18–22 August 2006. The gas was released from a point source up-stream of the base tower; three separate release points, each 1.5 m above the ground, were used at various times (Fig. 1a). The release rate was regulated by a mass flow controller (FC-260, Mykrolis Corporation, Billerica, MA, USA). At the release site in 2005, a 3-D sonic anemometer (SATI/3K, Applied Technologies, Inc. Longmont, CO, USA) at 1.5 m monitored wind speeds and turbulence. The data from the 3-D sonic anemometer and the mass flow controller were recorded at 10 and 1 Hz, respectively, by a laptop computer.

Sequential 5 min average concentrations of SF_6 were measured during each release at seven locations on and near the base tower using an automated bag sampling/analysis system developed at Washington State University and described by Flaherty et al. (in press). This system fills seven Tedlar bags at a steady rate for 5 min, while a second set of bags is automatically analyzed with a custom-built continuous SF_6 analyzer based upon electron capture detection (Benner and Lamb, 1985; Lamb et al., 1995). Once analyzed, bags are then evacuated in preparation for filling during the subsequent sample period. Each analysis period includes measurements of zero and span gas standards (Scott-Marrin, Inc., ±5% certified accuracy). The 7 sampling locations were selected from a total of 11 possible locations (5 on the

tower (5, 7, 10, 20 and 30 m) and 3 on each side slope). The sampling locations on the north- and south-facing side slope followed bearings of 210° and 30°, respectively. The sampling locations on the south-facing slope were 6.3, 10 and 17 m above the base of the tower and were 14, 20 and 31 m horizontally away from the tower, respectively. The sampling locations on the north-facing slope were 6.1, 8.3 and 10 m above the base of the tower and were 21, 26 and 29 m horizontally away from the tower, respectively. Concentrations of CO_2 in the sample bags were measured concurrently with the SF_6 measurements using an infra-red gas analyzer (Li-6262, Li-Cor Inc.). All the data from the SF_6 and CO_2 analyzers were stored at 1 Hz on a desktop computer. During the SF_6 release, two additional 3-D sonic anemometers (SATI/3K, Applied Technologies, Inc.) were added to the base tower at 5 and 20 m. Measurements from these 3-D sonic anemometers were recorded at 10 Hz by a laptop computer.

2.5. CO_2 and SF_6 flux estimates

To estimate the mass balance at night for CO_2 and SF_6, we extended the method initially described by Pypker et al. (2007) in which the watershed is treated as an open cuvette. Finnigan et al. (2003) presented the mass balance equations applicable to surface-atmosphere exchange in a representative Cartesian control volume of height h over a patch of *horizontal* landscape with surface area A. They wrote flux equations for the volume by integrating the instantaneous mass balance at a point

$$\frac{\partial c}{\partial t}+\frac{\partial uc}{\partial x}+\frac{\partial vc}{\partial y}+\frac{\partial wc}{\partial z}=S(\mathbf{x})\delta(\mathbf{x}-\mathbf{x}_0) \quad (1)$$

where c is concentration, u, v and w are velocity components along the directions x, y and z, respectively (conventionally representing the downwind, cross-wind and vertical directions), t the time and the source term S, a function of the position vector $\mathbf{x}$ with components x, y and z, is multiplied by the Dirac delta function to signify that the source strength is zero except at the ground, where the position vector is $\mathbf{x}_0$. The integration is calculated horizontally over area A, vertically over height h and is averaged over time. *Over horizontal surfaces* it is then usually assumed that the time-averaged horizontal gradients of $\overline{uc}$ and $\overline{vc}$ are zero, and horizontal variation in mean vertical flux is negligible, so that the (one-dimensional) mass balance for the volume is given by

$$\int_0^h \frac{\overline{\partial c}}{\partial t}\,\mathrm{d}z+\overline{wc}(h)=\bar{S} \quad (2)$$

where $\bar{S}$ is the area- and time-averaged surface source strength. Eq. (2) forms the basis for many reported estimates of $\bar{S}$ for ecosystems in which the above assumptions are valid. However, over the steeply sloping terrain in this study, the assumptions that lead from the mass balance at a point (Eq. (1)) to the one-dimensional mass balance for a landscape patch (Eq. (2)) are clearly not valid. In particular, the advective flux in the down-valley direction is large during nocturnal drainage flow. Fig. 1a shows that the valley extends in a NW direction from a ridge-line at the SE, and has a V-shaped profile that narrows as the valley descends. Fig. 1b is a simplified version of the drainage flow profile used in the following flux estimations. The control volume is treated as a wedge with a horizontal 'lid', and blocked at its upper end. We assume that cross-valley (y axis) flux divergence is negligible, and that the ridge at the SE blocks any advective flow in the x direction from entering the upper end of the valley. Consequently, the only advective terms are subsiding vertical flow into the volume, at mean velocity w over the area A_e, and flow in the x direction leaving the valley through a triangular area A_o. The mass balance for the valley volume V, is

$$\int\int\int_V \frac{\partial \bar{c}}{\partial t}\,\mathrm{d}x\,\mathrm{d}y\,\mathrm{d}z = \int\int_{A_e} \overline{wc}_e\,\mathrm{d}x\,\mathrm{d}y+\bar{R}-\int\int_{A_o}\overline{u_o c_o}\,\mathrm{d}y\,\mathrm{d}z \quad (3)$$

where overbars signify time-averaging, $\bar{c}(x,y,z)$ is the CO_2 concentration in the valley, $\overline{c_o}(x_o,y,z)$ and $\overline{u_o}(x_o,y,z)$ the CO_2 concentration and down-valley wind speed, respectively, in the cross-section at the outlet location (x_o), $\overline{c_e}(x,y,z_e)$ the concentration of CO_2 entering the volume at height z_e and $\bar{R}$ is the flux of respired CO_2 averaged over the ground area of the volume. Each term in (3) can be expressed in units of mol s^{-1}.

Eq. (3) provides a method for estimating $\bar{R}$ if the advective and storage terms can be estimated. The equation can also be used for mass balance calculations of the inert tracer gas sulfur hexafluoride (SF_6) released in the watershed, but in this case there is assumed to be no external subsidence input of SF_6 into the volume.

In applying Eq. (3), we used 30 min mean wind speed, temperature and CO_2 concentration data collected on the base tower at the valley outlet. We made the following assumptions:

(1) The mean air temperatures and CO_2 concentrations observed at height z_r on the tower ($0 < z_r < h$, where h is tower height) were applicable throughout the outlet cross-section at the same height (i.e. a

horizontal homogeneity assumption (King, 1989) discussed later).

(2) Wind speeds in the air above the cold air drainage flow were negligibly small, i.e. horizontal advection was predominantly in the drainage flow measured on the tower. This assumption is discussed later.

(3) Because of drag forces near the side-slopes of the valley, mean wind speeds observed at height z_r in the drainage flow decreased in the cross-wind direction (y) according to a parabolic equation that Dobosy et al. (1989) used to describe nocturnal drainage flow in the Brush Creek Valley, Colorado. We calculated the dependence of wind speed $u(x_o, y, z_r)$ on y as:

$$\bar{u}(x_o, y, z_r) = \bar{u}(x_o, 0, z_r)\left\{1 - \left[\frac{y}{y_{max}(x_o, z_r)}\right]^2\right\} \quad (4)$$

where y_{max} (x_o, z_r) is horizontal distance from the tower to the side slope at height z_r.

(4) The storage term (the LHS of Eq. (3)) could be approximated by the difference between vertical concentration profiles observed at the base tower in CO_2 concentration profiles over 30 min averaging periods multiplied by the volume of the drainage flow. This approximation was discussed by Finnigan (2006), who suggested that it may significantly underestimate storage at traditional, horizontal flux sites when the in-canopy CO_2 concentration is influenced by low frequency incursion of large turbulent eddies from above the canopy. In our situation, a strong nocturnal inversion at the canopy top is likely to reduce this error.

(5) The subsidence flow at all points across the 'lid' of the valley consisted of air with CO_2 concentration c_e = 370 ppm corresponding to the regional background value. The mean subsidence velocity $\bar{w}$ across the 'lid' was estimated by equating the first term on the RHS of Eq. (3) to a virtual advective flux at the outlet cross-section of CO_2 at background concentration c_e, i.e.

$$\overline{wc_e} = A_e^{-1}\int_{A_o}\int \overline{u_o c_e}\,dy\,dz,$$
$$\text{i.e. } \bar{w} = A_e^{-1}\int_{A_o}\int \overline{u_o}\,dy\,dz \quad (5)$$

To evaluate the horizontal advective term in Eq. (3) from our limited number of observations, we treated the vertical cross-section of the watershed at the base tower as six layers (0–6.5, 6.5–8.5, 8.5–15, 15–25, 25–37 and >37 m). Advection in the upper layer was assumed zero (assumption 2 above). The cross-sectional area for each layer at the tower location, A_i (m^2) ($1 \le i \le 6$) was estimated using a digital elevation map in a GIS. For the midpoint (at height z_i) of each of the five lower layers, using 30 min averages from the tower profiling system, we determined the mean windspeed at the tower, $\overline{u_i}$ ($m\,s^{-1}$), mean air temperature, $\overline{T_i}$ (K), and calculated the mean concentration of CO_2, $\overline{c_i}$ ($mol\,m^{-3}$) from the observed CO_2 molar mixing ratio and the Gas Law using observed temperature and assuming a pressure of 95.6 kPa. Assuming that the air temperature and CO_2 concentrations were representative throughout a layer i but that the wind speed decreased in the cross-wind direction (see assumptions above), we estimated the windspeed variation in each layer as follows to allow for the asymmetric shape of the outlet cross-section. On each side of the tower a layer was treated as four adjoining elements with cross-sectional area (A_{ij}) ($-4 \le j \le 4$). The elements with $j = -1$ and $j = +1$ each represented 50% of the distance from the tower to the left and right valley side slopes, respectively; the remaining three elements on each side each represented 16.7% of the distance to the side slope. Windspeeds calculated for the center of each element were applied to the entire element. The term $\int\int_{A_o} \overline{u_o c_o}\,dy\,dz$, representing the advected output flow rate of CO_2, F_o ($mol\,s^{-1}$), is then approximated by

$$F_o = \left(\sum_{i=1}^{5}\overline{c_i} \times \left[\sum_{j=-4}^{4} u_{ij}A_{ij}\right]\right) \quad (6)$$

The storage term $\int\int\int_V \partial\bar{c}/\partial t\,dx\,dy\,dz$ (called F_{store} from now on) was calculated by assuming that the change in CO_2 concentration measured in each layer i at the tower over a period Δt from $t-1$ to t represented the storage in that layer within the valley volume. We assumed that: (1) the change in concentration in the top layer (with no advective flow) was negligible. (2) Storage only occurred between 0 and 37 m from the forest floor as a strong inversion likely existed above the canopy. Hence:

$$F_{store} = \frac{\sum_{i=1}^{5}(\bar{c}_{i,t} - \bar{c}_{i,t-1})V_i}{\Delta t} \quad (7)$$

where V_i is the volume of the layer.

The mean subsidence velocity $\bar{w}$ was estimated from Eq. (5) using the layer approximation method described for the advective flux, and the rate of entry of CO_2 into the valley by subsidence is then given, from Eq. (3), by $F_e = \bar{w}c_eA_e$.

To assess the validity of the method of estimating net advection of CO_2 we also applied the model to data collected during the release of SF_6 below the canopy. On 14 September 2005, both SF_6 and CO_2 concentrations were monitored at the base tower during a period when there was below-canopy drainage flow. During this period, the SF_6 was stratified, and was largely contained below the canopy top because of a strong temperature inversion at the canopy top. The flow rate of SF_6 out of the watershed was estimated using a method similar to the one outlined above, with all variables using CO_2 concentrations being replaced by the SF_6 concentrations. There were two notable exceptions: (1) we assumed that F_i was zero because SF_6 concentrations are negligible in the background atmosphere and (2) we assumed that SF_6 storage in the canopy was zero, since the release rate was constant and it required approximately 30 min for the plume of SF_6 to decline to zero after the SF_6 was no longer being released (data not shown). The flow rate of SF_6 observed to advect from the watershed was compared to the actual release rate for the period where the SF_6 was confined below the top of the canopy because of the temperature inversion (Fig. 2).

2.6. Data analysis periods

Climatological (wind speed, wind direction and temperature) were collected throughout 2005 and 2006, and four summer sampling periods (28–29 June, 20–21 July, 10–11 August and 17–18 August 2005) were selected for detailed analysis. These nights spanned the summer and are representative of the typical weather conditions during this season. For each period, potential air temperature at the tower (Fig. 2), wind speeds and wind direction at the tower (Figs. 3 and 4), and changes in potential air temperature with elevation along the valley (Fig. 7) were calculated. Using the observations, bulk Richardson numbers in the trunk space below the canopy foliage (Fig. 8) and CO_2 concentrations/fluxes passing the tower (Figs. 9 and 11) were also calculated. To assess the seasonal frequency of drainage flow we analyzed wind direction data from the base tower in 2005 (Fig. 5).

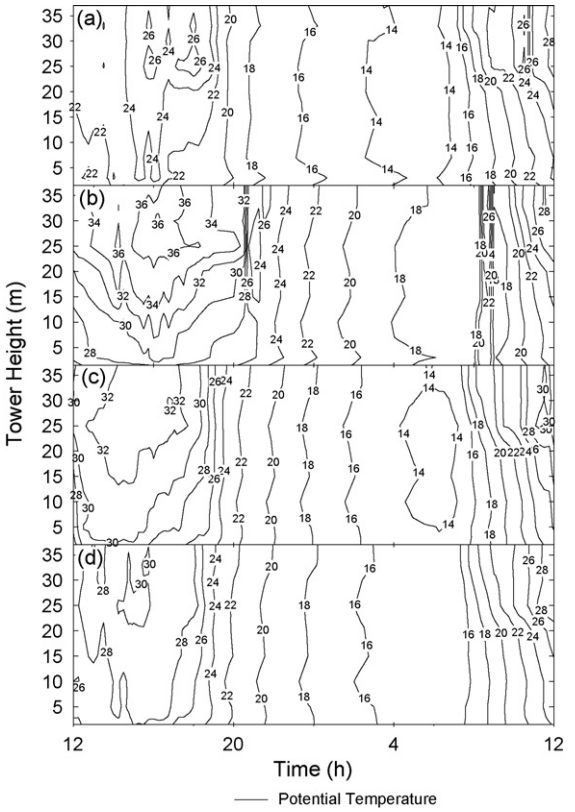

Fig. 2. Diel changes in the vertical profile of potential temperature at the 37 m base tower. Diel profiles are presented for: (a) 28–29 June, (b) 20–21 July, (c) 10–11 August and (d) 17–18 August 2005.

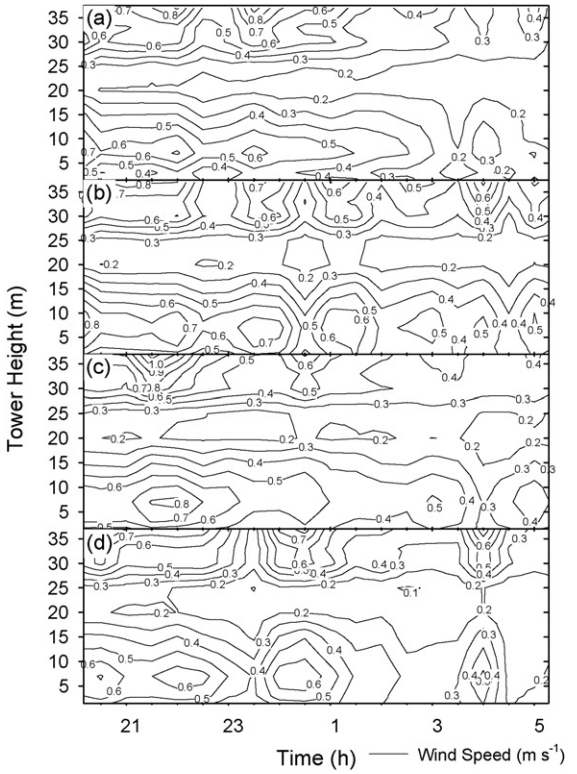

Fig. 3. Nocturnal changes in windspeeds at different heights on the 37 m base tower. Profiles are presented for: (a) 28–29 June, (b) 20–21 July, (c) 10–11 August and (d) 17–18 August 2005. From 20:00 to 5:00 h, cold air drainage was occurring at all heights on each sample date.

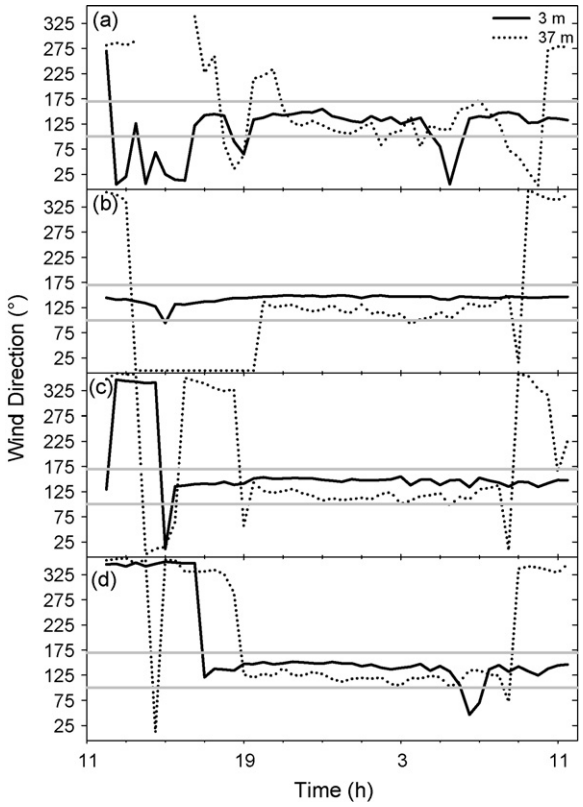

Fig. 4. Diel changes in wind direction at the bottom (3 m) and top (37 m) of the base tower for sample periods in 2005. Down-valley flow is occurring when the black line is in between the two gray lines. The wind directions at the bottom and top of the tower are presented for: (a) 28–29 June, (b) 20–21 July, (c) 10–11 August and (d) 17–18 August 2005.

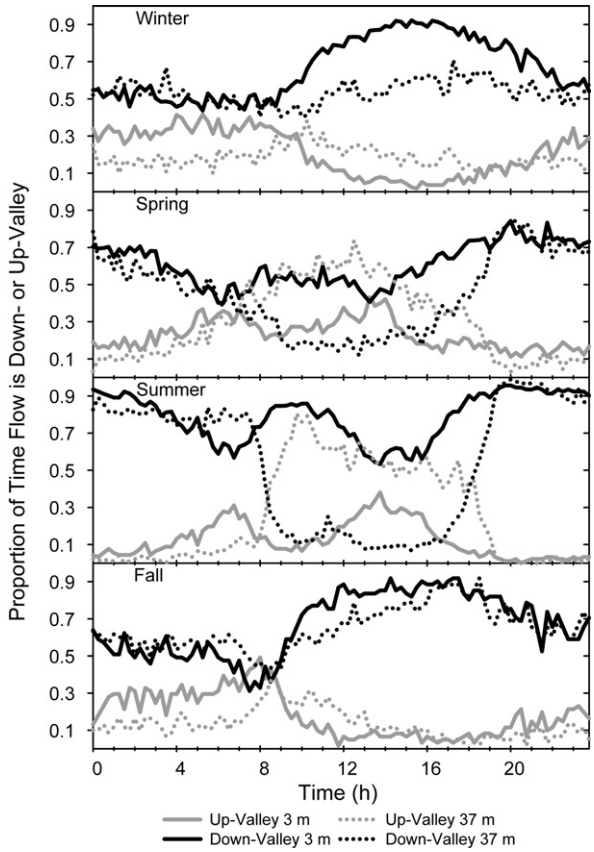

Fig. 5. Seasonal changes in the diel wind direction at the 37 m base tower in 2005. The seasons were divided into Winter (December, January, February, March), Spring (April, May, June), Summer (July, August, September) and Fall (October, November).

Data from SF_6 releases in 2005 and 2006, together with tethersonde and sodar measurements (2006 only), were analyzed to estimate advective flow and mass balance. Representative results are presented in Figs. 6, 10 and 12.

3. Results

3.1. Diel variation of the vertical profile of temperature at the base tower

Throughout the summer months, the vertical temperature profile at the base tower varied in a similar pattern each day (Fig. 2). During daylight hours, solar radiation was absorbed by foliage on the trees (between 20 and 30 m height), so that by mid-afternoon the potential temperature of the air within the foliage airspace was 2–6 °C higher than that of air below the tree foliage. This heating created a strong temperature inversion in the airspace between the ground and the base of the canopy foliage (at roughly 20 m). As the sun set, the canopy top cooled radiatively, so that the gradient in potential temperature of the air below the canopy top approached zero between 18:00 and 20:00 h (Fig. 2). However, in some instances a pocket of cold air remained near the ground (Fig. 2) in the region with the greatest below canopy wind speeds (Fig. 3). Throughout the night (20:00–6:00 h), the vertical temperature profile on the tower remained nearly neutral. After sunrise, the foliage began absorbing solar radiation and the cycle continued.

3.2. Variation of wind speed and direction at the base tower

The velocity of the cold air drainage typically decreased at all heights on the base tower as a night progressed (Fig. 3). At 20:00 h, when the cold air drainage was occurring at all heights (Fig. 4), there was usually a maximum wind speed at approximately 5 m

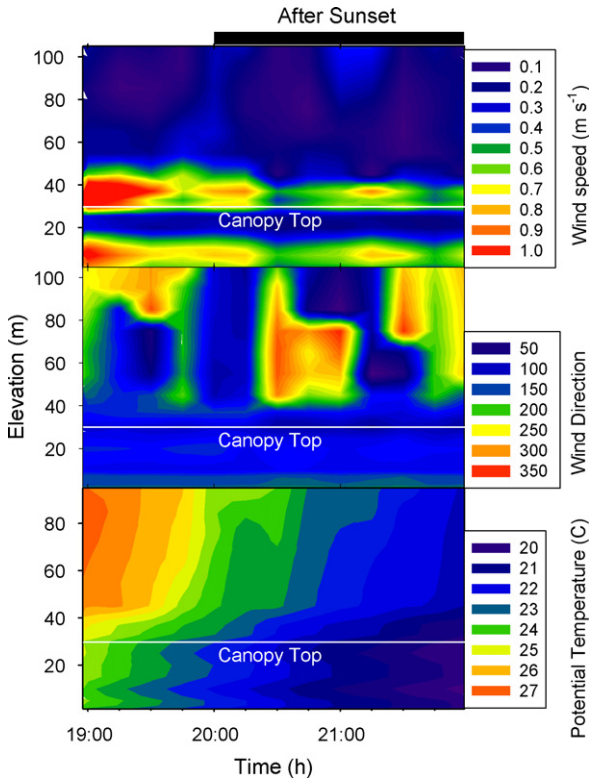

Fig. 6. Diel changes in the vertical wind speed (a), wind direction (b) and potential temperature (c) profiles in the valley on 21 August 2006.

(Fig. 3). The decrease in wind speeds below and above 5 m was presumably caused by frictional drag at the ground and from the tree boles/branches and foliage, respectively. Wind speeds above the canopy were usually greater than within the foliage layer (Fig. 3).

The wind directions at the bottom and top of the base tower varied both through the day and seasonally (Figs. 4 and 5). During the summer, nocturnal cold air drainage was common, and the down-valley wind direction (≈140°) frequently persisted all day beneath the canopy. Down-valley flow *above* the canopy usually began after net radiation above the canopy approached zero provided that synoptic windspeeds were low (Pypker et al., 2007). Nocturnal cold air drainage usually persisted throughout the night, but was observed slightly less frequently between 24:00 and 05:00 h (Fig. 5).

From October to March, cloudy skies and precipitation are common in the Pacific Northwest (Taylor and Hannan, 1999). During these periods, nocturnal cold air drainage occurred less frequently than in summer due to the combined effects of decreased radiation, shorter days and persistent cloud cover. In spring (April–June), cloud cover and rainfall usually decrease. However, during spring 2005 these months were exceptionally wet, resulting in the canopy receiving less solar radiation than normal (data not shown); nocturnal cold air drainage occurred only between 60% and 80% of the time (Fig. 5).

3.3. Tethersonde and sodar profiles of wind speed, direction and temperature

Data in Fig. 3 suggest that there may have been significant drainage flow occurring at night above the maximum level of tower measurements (37 m). Measurements from the sodar and tethersonde during typical summer evenings in August 2006 allowed us to investigate the structure of the air flow up to about 100 m. Fig. 6, which was constructed by combining tower, tethersonde and sodar measurements, illustrates the profiles of wind speed, direction and temperature observed in and above the canopy on 21 August 2006. Similar structure was observed on other nights, supporting the generality of this pattern in summer. The figure demonstrates that there were two distinct jets, separated by a region of low windspeed in the foliage zone. The upper jet extended to 40–50 m, and was consistently down-valley. Above this level, wind speeds were very low, and wind direction was variable.

3.4. Spatial variation in the watershed of diel air temperature near the ground

The spatial variability of potential temperature near the ground (0.5 m) within the watershed also varied with a diel cycle (Fig. 7). During the day, the potential temperature at the top of the watershed was usually slightly higher than that at the bottom of the watershed. The cooler temperatures in the lower valley likely occurred because the lower valley received less direct solar radiation due to shading of the steep valley walls. As the day progressed and the sun set, the potential temperature variation along the transect that extended approximately up the valley axis tended to zero between 18:00 and 20:00 h (Fig. 7). After 20:00 h, a temperature inversion formed within the watershed that persisted until approximately 06:00–08:00 h, when direct solar radiation was once again absorbed.

On most nights, the temperature inversion within the watershed was well developed by 22:00 h (Fig. 7). The rate of change of potential temperature with elevation was smaller below about 700 m than above 700 m early in the night, but became increasingly constant as the night progressed. Between 20:00 and 03:00 h, the inversion was well developed and potential temperature changed almost linearly with height.

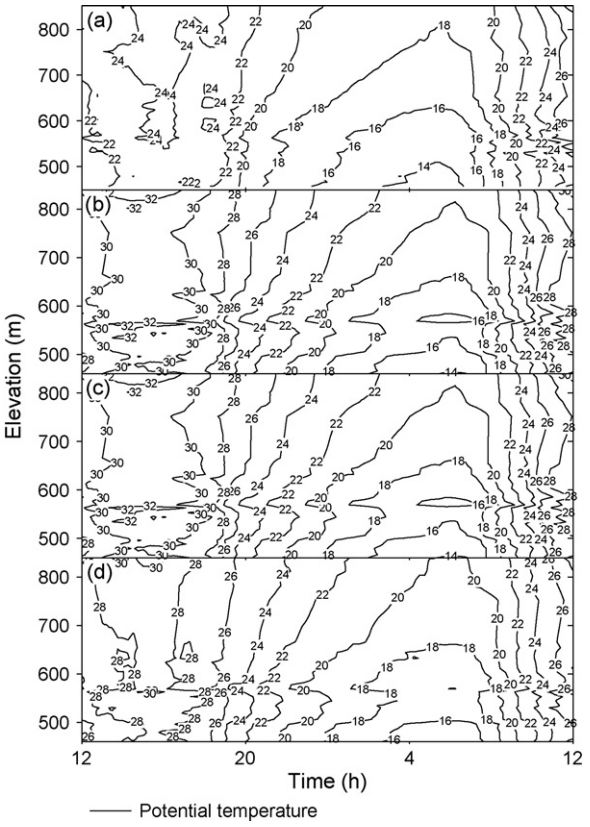

Fig. 7. Diel changes in potential temperature along the axis of the watershed. Diel profiles are presented for: (a) 28–29 June, (b) 20–21 July, (c) 10–11 August and (d) 17–18 August 2005.

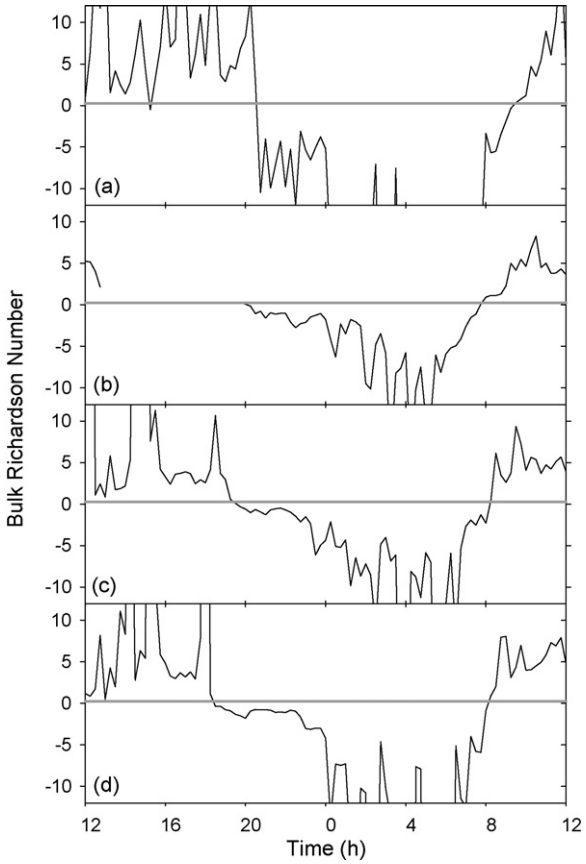

Fig. 8. The bulk Richardson number at the base tower for four nights during 2005. The bulk Richardson number was calculated using air temperature and windspeeds measured at 3 and 20 m (below the canopy foliage) for: (a) 28–29 June, (b) 20–21 July, (c) 10–11 August and (d) 17–18 August 2005. The gray line indicates the theoretical critical gradient Richardson number for transition from non-turbulent to turbulent flow (0.25). A portion of the data from 20 to 21 July is missing because of a malfunctioning anemometer.

3.5. Turbulence and stability below the canopy

In stratified flow near the surface, turbulence is generated by vertical wind shear and by pressure fluctuations caused by the form and viscous drag of roughness elements such as foliage, branches and stems. Turbulence can persist only if these processes are sufficiently strong to overcome the buoyancy forces associated with thermal stratification (Mahrt, 1986). The onset of turbulence is often estimated from the gradient Richardson number; values of $Ri < 0.25$ are sometimes used to define conditions when turbulence is likely to persist (Stull, 1988). Fig. 8 shows bulk Richardson numbers calculated using air temperature and windspeeds measured at 3 and 20 m (below the canopy foliage). The air flow below the canopy was usually turbulent during the night (negative *Ri*) and stratified during the day (positive *Ri*). The *Ri* usually switched from below or above the critical value of 0.25 near sunrise and sunset, respectively. (Strictly this critical value applies to the gradient Richardson number; bulk *Ri* calculated over finite layers is a less sensitive measure of the tendency for turbulence, but Fig. 8 shows a very clear shift in *Ri* at these times.)

During the night, the potential temperature near the ground was slightly warmer than in the canopy, generating thermal instability and supporting turbulence; in contrast, turbulence was suppressed during the day, when a strong inversion typically formed below the canopy and maintained stratified flow (Fig. 2).

3.6. Nocturnal CO_2 concentrations at the base tower

During summer, CO_2 concentrations measured on the tower had a consistent diel pattern (Fig. 9). During the day, the vertical CO_2 concentration was stratified, with the greatest concentrations near the ground.

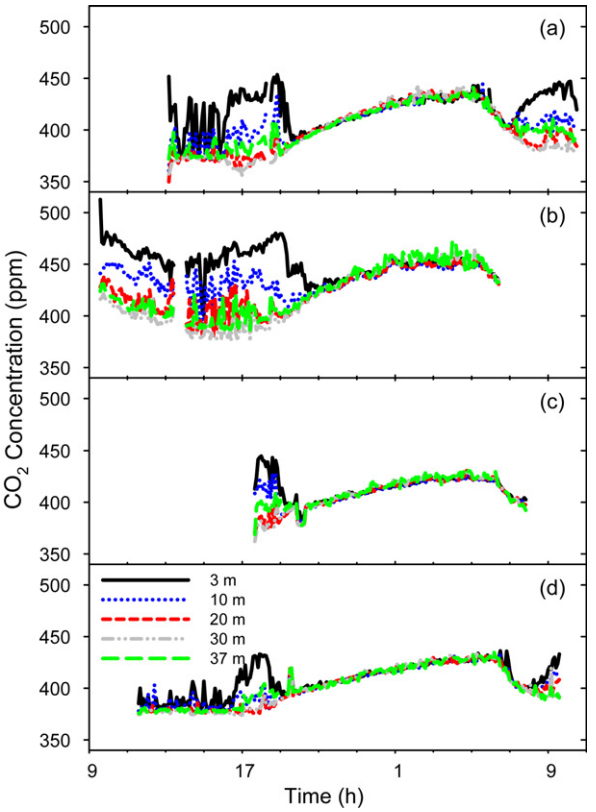

Fig. 9. Variation of CO_2 concentration with time at five heights on the base tower for four nights during 2005. The CO_2 profiles are presented for: (a) 28–29 June, (b) 20–21 July, (c) 10–11 August and (d) 17–18 August 2005.

However, in the early evening, as the vertical gradient in potential temperature approached zero (Fig. 2) and the air below the canopy became turbulent (Fig. 8), the vertical gradient in CO_2 concentration also approached zero. At this point, air was flowing down-valley at all heights (Fig. 4) and appeared well mixed (Fig. 9). At sunrise, the air remained well mixed, with CO_2 concentrations similar at all heights on the base tower. However, despite the CO_2 remaining well mixed for about 2 h after sunrise, its concentration decreased, until between 07:00 and 08:00 h when a large portion of the watershed began to receive inputs of direct solar radiation. After this time, the foliage airspace increased in temperature relative to the air below the canopy (Fig. 2), creating a stable temperature profile below the foliage layer, and the CO_2 concentrations again became stratified (Fig. 9).

3.7. SF_6 concentrations at the base tower

The SF_6 concentration profiles (Fig. 10) measured on the tower followed a similar diel pattern as the CO_2 concentration profiles (Fig. 9). In the afternoon, the SF_6 concentrations were strongly stratified, with the greatest concentrations near the ground and smallest just above the canopy. However, around sunset, when the air below the canopy became well mixed, SF_6 concentrations at all heights began to decrease and converge. The mixing of the SF_6 coincided with the bulk Richardson number dropping below 0.25. After about 18:00–18:30 h, the SF_6 concentrations varied relatively little with height, but, unlike the CO_2 profiles (Fig. 9), the concentrations of SF_6 were still greatest near the ground. We believe that this imperfect mixing occurred because SF_6 was released from a single point source near the ground, whereas respired CO_2 is released from the soil and all levels in the canopy throughout the watershed.

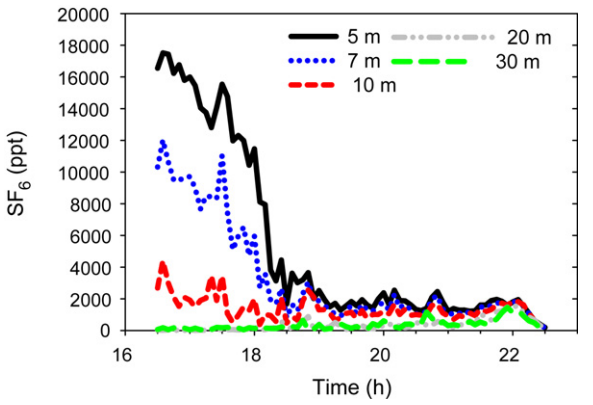

Fig. 10. Variation with time of SF_6 concentrations at five heights on the 37 m base tower from 17:00 to 23:00 h on 14 September 2005.

Most of the SF_6 release experiments were conducted with the release point about 600 m upstream of the base tower near the watershed axis or on the valley side-slopes. However, when the SF_6 release point was located near the ridge at the head of the watershed (see Fig. 1a), the gas was also readily detected at the base tower at night after a delay corresponding to an advection speed of 1–2 m s^{-1}, confirming that air flow from the limits of the watershed was being channeled through the narrow valley outlet at the base tower.

3.8. Mass budgets of SF_6 and CO_2

Fig. 11 shows the mean respiration rate, $\bar{R}$, in the watershed for four nights in 2005, estimated as the residual after using Eqs. (3)–(7) to determine the mean subsidence velocity, horizontal advective output flux and storage, confining the integrations to heights below that of the tower (37 m). The subsidence velocity (calculated using Eq. (5)) declined from 0.18 cm s^{-1} early in the evening to 0.04 cm s^{-1} near sunrise. The

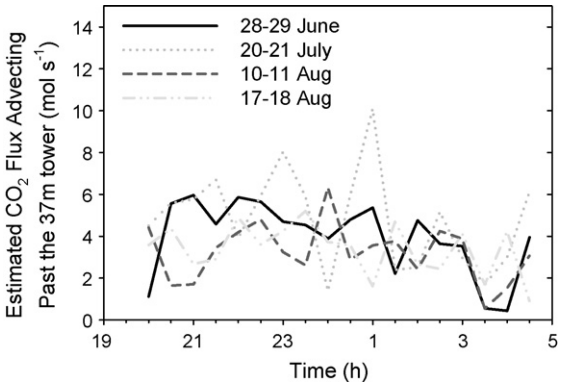

Fig. 11. Estimates of the CO_2 respired within the watershed based on mass balance calculations for observations on four nights in 2005: 28–29 June, 20–21 July, 10–11 August and 17–18 August 2005.

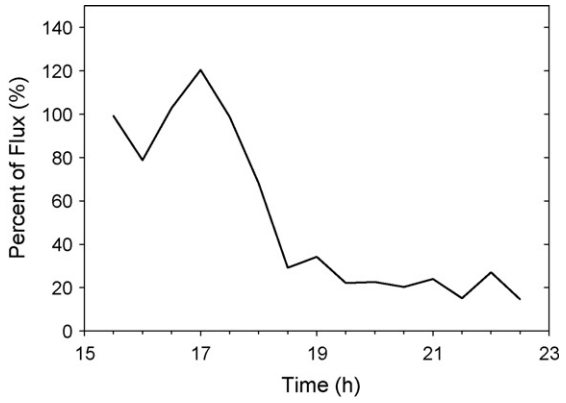

Fig. 12. Estimates of SF_6 advection below the top of the 37 m base tower. The fluxes were estimated from the mid-afternoon when the SF_6 was entirely contained within the drainage below the canopy, to late evening when a second drainage flow (not included in these calculations) had developed above the canopy.

decline resulted from declining windspeeds as the evening progressed (Fig. 3). These values are smaller than the range 0.2–5.4 cm s^{-1} reported by Carlson and Stull (1986) in a nocturnal boundary layer in Oklahoma, perhaps because of the limited integration height. The value of $\bar{R}$ based on estimations of flow exiting the valley at heights below the tower ranged between 0.4 and 11 mol s^{-1} with a nightly mean flow rate of 3.2–5.2 mol s^{-1} (Fig. 11). Expressed per unit floor area of the valley (96 ha) the mean ecosystem respiration rate corresponds to 3.3–5.4 μmol m^{-2} s^{-1}. The flow rate of CO_2 passing the tower fluctuated with changing CO_2 concentrations and decreasing windspeeds. As the night progressed, the increasing CO_2 concentrations (Fig. 9) partially offset the declining windspeeds (Fig. 3), thereby maintaining the quantity of CO_2 advecting past the tower relatively constant (Fig. 11).

Flow rates of SF_6 past the base tower were estimated in the same manner as the CO_2 flow rates. However, unlike CO_2, the quantity of SF_6 released in the watershed was known. Thus, the proportion of released SF_6 advecting below the top of the tower could be calculated (Fig. 12). In the late afternoon, when the drainage flow was confined below the canopy, estimates of the rate of SF_6 advection were within about 20% of the release rate of SF_6. This close agreement in view of the approximations adopted supports our assumptions in the mass balance calculations. However, after sunset, only 20–25% of the SF_6 released was estimated to advect between 0 and 37 m. This change coincided with the inversion below the canopy dissipating and the airflow becoming turbulent. The data of Fig. 6 suggest that, with no thermal stability to suppress mixing, the SF_6 was also advected in the upper jet that developed between the canopy top and about 45 m. Preliminary estimates using observed mean windspeed in the upper jet and assuming that the SF_6 concentration was constant throughout the jet indicate that this scenario could account for all the SF_6 released, but further measurements of SF_6 in the upper jet are needed.

4. Discussion

4.1. Flow characteristics

The wind patterns in this valley are typical for mountainous terrain, with katabatic (cold air drainage) flow occurring on clear, calm nights and anabatic (up-valley) flow sometimes occurring during the day. The anabatic flow was usually restricted to above the canopy (Fig. 4), but sometimes occurred both above and below the canopy (data not shown). In general, the flow dynamics can be separated into four categories as defined by Whiteman (1990): daytime flows, evening transition, nighttime conditions (formation of a cold air pool) and morning transition.

4.1.1. Daytime flows

In summer, down-valley drainage frequently occurred all day below the canopy (Figs. 4 and 5). When down-valley drainage ceased during the day, it usually resumed again at the lowest levels on the base tower 1–2 h before cold drainage occurred at all heights on the tower (Fig. 4). The afternoon cold air drainage was stably stratified (Fig. 2) and was usually limited to the trunk space below the canopy foliage (Fig. 5). In the spring and summer, the most common time for up-valley flow below the canopy was in the afternoon when air temperatures were the greatest. It is not unusual for a mountain valley to have down-valley flow near the

surface and up-valley flow aloft (Hawkes, 1947; Whiteman, 1986, 1990). During the day, heating in the valley results in a pressure gradient between the watershed and the adjacent larger landscape which promotes up-valley flow (Nikus and Vergeiner, 1984). However, unlike the situation for bare ground, where short and long wave radiation exchanges take place at the soil surface, in forested ecosystems most of the radiation is exchanged at the top of the tree canopy. Because the dense canopy intercepted most of the incoming solar radiation, a stable layer frequently formed beneath the canopy during the day (Fig. 2) that resulted in stratified flow below the canopy (Fig. 9).

The stable layer beneath the canopy had limited mixing with the air above. During the tracer experiment on 14 September 2005 there was cold air drainage below the canopy during the day. During this period SF_6 remained stratified in the sub-foliage-layer air space, with very little SF_6 detected above the canopy (Fig. 12). On other summer days, the air below the canopy flowed either down-valley or up-valley during the day (Figs. 4 and 5). For example, the daytime wind direction at 3 m was up-valley for part of the day on 17–18 August, but down-valley all day on 20 July 2005. Differences in wind speeds and temperatures throughout the watershed may explain these variable flow patterns. The potential temperature at 3 m elevation on the base tower averaged 6.0 and 1.8° cooler than at 3 m on the ridge tower from 11:00 to 17:00 h on 20 July and 17 August 2005, respectively. The smaller temperature difference on 17 August 2005 indicates that air within the watershed was less strongly stable. On both days, the wind direction at the top of the towers was northwest. However, windspeeds at 23.5 m on the ridge tower were larger on 17 August than on 20 June 2005 (2.3 and 1.8 m s^{-1}, respectively). The smaller temperature difference and greater wind speeds on 17 August may have allowed winds above the canopy to penetrate into the canopy, thereby forcing the wind up-valley (Whiteman, 1990). It thus seems likely that daytime variability in valley flow depends of the strength of synoptic flow and other large- and meso-scale phenomena.

4.1.2. Nighttime transition

If cold air drainage was not already occurring, it usually began below the canopy between 16:00 and 18:00 h (Fig. 4). As reported elsewhere, the shallow drainage that occurred beneath the canopy rapidly increased in depth when net radiation above the cooling surface became negative (e.g. Pypker et al., 2007; Whiteman et al., 1989) and the vertical profile of potential temperature in the canopy became isothermal (Fig. 2). The nighttime transition was characterized by having the greatest windspeeds of the evening (Fig. 3).

Because the air below the canopy was no longer stably stratified, the air became well mixed through turbulence generated by stems and foliage as demonstrated by the change in CO_2 and SF_6 profiles (Figs. 9 and 10). During the day, when the temperature profile was stable, the CO_2 and SF_6 profiles were stratified, but when the profile became nearly isothermal the CO_2 and SF_6 were mixed throughout the canopy air-space because the cold air drainage was turbulent.

During the evening transition, the depth of the cold air drainage appeared to rise above 37 m (the highest measuring point), and the tethersonde and sodar measurements in 2006 confirmed this (Fig. 6). Prior to the evening transition, very little SF_6 was detected at the top of the tower and estimates of SF_6 advection in the sub-canopy flow closely matched release rates (Fig. 12). However, in the well-mixed flow after the transition, only 10–20% of the SF_6 released could be accounted for in the flow below the tower. Rough calculations (data not shown) support the assumption that the remaining 80–90% of the release was then advecting in an upper cold air drainage jet extending from the canopy top to about 45 m, as revealed by sodar and tethersonde data.

4.1.3. Nighttime flow and the formation of a cold air pool

In the evening, often between 20:00 and 2200 h, the temperature profile within the watershed became stably stratified (Fig. 7) and the temperature gradient along the axis of the watershed usually declined nearly linearly with height. The data suggest that a cold air pool formed, extending to an altitude of about 850 m. The cold pool usually persisted until the morning when convection resulting from the absorption of solar radiation broke the inversion in the valley (Figs. 2 and 7). The formation of the cold air pool was accompanied by decreasing windspeeds and periods where the wind at the base tower was weak and swirled from multiple directions. These periods of low windspeeds account for approximately 80% of the nocturnal periods when the air was not flowing down-valley.

Past research has demonstrated that cold air pools form in most valleys that experience cold drainage (e.g. Clements et al., 2003; Iijima and Shinoda, 2000; Magono et al., 1982; Maki and Harimaya, 1988; Mori and Kobayashi, 1996; Yoshino, 1984). However, the depth and strength of the inversion layer depends on whether the valley is closed or open at the base

(Clements et al., 2003). The valley in this study is open, and drainage continued through the night (Figs. 3 and 4). Upon forming a cold air pool, air flow through the pool usually continues as long as a drainage outlet exists (e.g. Iijima and Shinoda, 2000; Magono et al., 1982; Maki and Harimaya, 1988; Mori and Kobayashi, 1996; Yoshino, 1984).

The size of the pool is likely influenced by the surrounding topography. When a small watershed drains into a larger watershed with its own cold air pool, the depth of the pool in the small watershed becomes a function of the depth of the pool in the large watershed (e.g. Mori and Kobayashi, 1996; Neff and King, 1989). Our watershed drains to the north into the larger Lookout Creek which then flows into the Blue River watershed (Fig. 1a). Neff and King (1989) also monitored the filling of a valley that was a tributary to a larger valley/drainage system. They reported that the cold air pool in the larger valley grew large enough to encompass the entire tributary valley. Our valley likely experiences the same phenomenon. In the early evening, a cold air pool forms rapidly and the inversion layer extends from the valley bottom to the ridge (Fig. 7). After this time, the depth of the cold air pool may be controlled by an air pool developing in the larger Lookout Creek airshed. Further work with a tethersonde and sodar is necessary to determine the depth of the cold air pool in this larger valley.

4.1.4. Morning transition

In the watershed, the temperature inversion near the ground persisted until after sunrise, usually requiring 1–2 h for the cold air pool to dissipate. The destruction of the inversion in a valley usually occurs because of two processes: the absorption of solar radiation at the ground that results in convection above the valley floor; and the descent of the top of the inversion layer (Whiteman, 1982). As our temperature sensors on the transect were only 0.5 m from the ground, they were capable only of detecting the destruction of the inversion near the ground. In general, the potential temperature above 650 m increased more rapidly with time than the potential temperature below 650 m during most mornings (Fig. 7). Regions that heated more rapidly were unlikely to contribute to the cold air drainage that was still occurring at the 37 m tower (Figs. 3 and 4). Hence, the CO_2 measured at the tower remained well mixed, but the concentration declined because the air contained respired CO_2 from a smaller fraction of the watershed. After the inversion layer was dissipated (Fig. 2), the temperature profile and CO_2 profile at the 37 m tower became stratified. If cold air drainage continued, it was then confined below the canopy (Fig. 4).

4.2. Implications for monitoring carbon isotopes within the cold air drainage

The different stages of flow provide both opportunities and challenges when monitoring the isotopic composition or concentrations of CO_2 in complex terrain. During the ‘‘daytime condition’’, there is an opportunity to monitor respiration below the canopy. When there was drainage flow, the air below the canopy was poorly coupled with the air above the canopy (Figs. 2 and 9). The strong inversion layer below the canopy limited the dispersion of gases entrained within the cold air drainage. Hence, the SF_6 and CO_2 concentrations were strongly stratified and most of the SF_6 released could be accounted for in the flow below the tower top. The observed poor dispersion of the SF_6 plume suggests that the net CO_2 flow rates observed at the tower was likely originating at this time from the riparian area of the watershed directly upstream of the tower. This riparian area consists mainly of broadleaved alder trees that are relatively well supplied with water throughout the summer.

Measurements of isotopes in CO_2 should probably be avoided during the nighttime transition. During this period, the depth of the cold air drainage is increasing and the footprint size of the tower is probably shifting from primarily the riparian area to a large fraction of the watershed. In complex terrain the ecosystem is not homogeneous. The isotopic composition of ecosystem respiration varies with plant species and microclimate (e.g. soil water availability, vapor pressure deficit) (Bowling et al., 2002; Buchmann et al., 1997; Ekblad and Högberg, 2001; Farquhar et al., 1989; Flanagan et al., 1996; Högberg et al., 2001). Hence, one would expect that shifts in the footprint area during this transition period would alter the Keeling plot slope and intercept because the signal from the respiration source was not constant.

The best time to collect air samples for Keeling plot analysis in this ecosystem appears to be between 20:00 and 03:00 h, after the formation of the cold air pool, when the temperature profile along the watershed transect declines linearly with distance, suggesting that the drainage encompasses the entire watershed. Past work has demonstrated that collecting air samples on the tower during this period provides a range of CO_2 concentrations that is sufficient to calculate the isotopic composition of ecosystem respiration (Pypker et al., 2007).

After sunrise, as the sun first strikes the walls of the upper valley, the footprint of the tower begins to shrink as portions of the watershed are no longer contributing to the cold air drainage, so sampling for isotopic analysis at the watershed scale is no longer possible. The decrease in the footprint of the tower is illustrated in the CO_2 concentration data (Fig. 9). After sunrise, the drainage remained well mixed but the CO_2 concentrations at the tower decreased, probably because, the absorption of solar radiation in upper portions of the watershed destroyed the local inversion (Whiteman, 1982; Whiteman et al., 2004) and eliminated the contribution of respired CO_2 from that region of the watershed.

4.3. Estimating nighttime ecosystem respiration

Measurements from a single vertical profile have been used successfully to estimate the flow rate of mass or energy out of a watershed (Dobosy et al., 1989), but the underlying assumptions frequently result in overestimates of the volume flux of air (King, 1989). To estimate fluxes using a single vertical profile, one must assume that the properties of cold air drainage are horizontally homogenous (King, 1989). This assumption is probably valid for CO_2 concentrations in the cold air drainage observed in this study at night because the drainage is well mixed (Fig. 9). Because wind speeds are usually maximum near the center of the watershed and decrease within the forest canopy (e.g. Allen, 1968; Fons, 1940; Landsberg, 1971; Shaw, 1977; Turnipseed et al., 2003), we adjusted the horizontal wind speeds using an equation provided by Dobosy et al. (1989).

During the SF_6 experiments, the rate of gas release in the watershed was known, so we could assess the accuracy of using a single tower measurement to quantify advective flow rates. During the afternoons of the releases, SF_6 was confined within the drainage flow below the canopy (Fig. 12). When calculating the SF_6 flow rates during these periods, our integration method estimated advective flow rates within about 20% of the SF_6 release rates. This is somewhat better than in other studies using this method, in which flow rates were overestimated by a factor of 1.5–2 (Dobosy et al., 1989; King, 1989). However, the lack of mixing of respired CO_2 at this time makes it impossible to know the area from which observed CO_2 advection is occurring, so CO_2 flux densities could not be determined during these periods.

At night, our data suggest that the entire watershed area is contributing to advected CO_2 leaving the valley cross-section at the tower. The nightly mean watershed-scale flux of respired CO_2 (R), based on tower observations below 37 m, ranged between 3.2 and 5.2 mol s^{-1} (Fig. 11). Past measurements in similar forests of the region, using small chambers over the soil, found that soil respiration could be up to 7 μmol m^{-2} s^{-1} (Campbell and Law, 2005; Harmon et al., 2004); observed summertime soil respiration in this watershed is usually around 3 μmol m^{-2} s^{-1} (Z. Kayler, unpublished). Given that soil respiration often represents about 70% of ecosystem respiration (e.g. Jiabing et al., 2006; Law et al., 2001; Valentini et al., 2000), the total nocturnal respiratory flux for the 96 ha watershed may be 4–10 mol s^{-1}. So estimates of watershed-scale $\bar{R}$ based on observations below 37 m account for 30–100% of the estimated ecosystem respiration (Fig. 11). However, the sodar and tethersonde indicate that significant advection also develops at night in a well-defined upper cold air drainage jet extending from the canopy top to about 45 m. Although, we were unable to collect SF_6 concentration data throughout this upper jet, it appears from extrapolation that most of the SF_6 advection (and by analogy, CO_2 advection) could be accounted for by transport in the above- and below-canopy jets. If this can be confirmed by extending the tower in future research, it seems likely that good estimates of advective fluxes could be obtained in this watershed, and consequently more precise nocturnal respiration rates could be estimated.

5. Conclusions

During spring, summer and fall, the cold air drainage in the steeply sloping, forested watershed followed a consistent diel pattern. During the day, the wind direction above the canopy was either up- or down-valley while the wind direction below the canopy was typically stratified and down-valley. During summer, up-valley flow below the canopy became more frequent in the late afternoon, presumably because of greater solar heating within the valley. Once the watershed was no longer receiving direct solar radiation, cold air drainage started below the canopy. After the vertical potential temperature profile at the base tower became nearly isothermal, drainage flow below the canopy became well-mixed. With negative net radiation at the canopy top, an inversion formed, and a second cold air drainage jet was established above the canopy, extending to 40–50 m. As the nocturnal drainage continued, a cold air pool frequently formed within the valley and deepened between 20:00 and 24:00 h. During this period, the cold air drainage continued, but as the night progressed the wind speed decreased. After sunrise, CO_2 in air draining past the tower remained

well mixed, but its concentration decreased. It is likely that during this period, a portion of the watershed was no longer contributing to the cold air drainage (and consequently was not contributing respired CO_2 to the air measured at the base tower) because it was receiving direct solar radiation that eliminated the local inversion.

The footprint of the base tower appears to encompass the entire watershed after the formation of the cold air pool in the valley. During this period, the potential temperature profile near the ground indicates that there is a strong inversion throughout the watershed. A parcel of air that starts at the top of the watershed is likely to cool rapidly and descend to the bottom of the watershed. Because the air is well mixed and the footprint of the tower is constant, it is probable that sampling at the tower during this period would provide valid estimates of respiration rates and carbon isotope discrimination at the watershed scale.

The current work demonstrates that a single vertical profile can provide estimates of carbon fluxes advecting laterally out of this watershed, and that nocturnal respiration fluxes deduced from mass-balance analysis are plausible in relation to likely ecosystem-scale respiration. However, these estimates are uncertain because of several assumptions involved. If more accurate estimates of CO_2 flow rates in valley air drainage are to be achieved, future work is needed to improve our ability to quantify spatial variability in wind fields within the valley and to investigate any entrainment exchange rate between overlying air and the cold air drainage jets.

Acknowledgements

We wish to thank J. Moreau, T. Cryer and C. Czarnomski for their help with site construction, fieldwork and data collection, T. Valentine for providing us with the cross-sectional area and surface are of the watershed, Will Rebmann for assistance with analyzing the data, C. Daly and J. Smith for modeling the solar radiation input to the watershed and C. Tarasoff for her helpful comments on the manuscript. Funding for this project was provided by the National Science Foundation (Grants DEB-0132737 and DEB-0416060).

References

Allen Jr., L.H., 1968. Turbulence and wind speed spectra within a Japanese larch plantation. J. Appl. Meteorol. 7, 73–78.

Anthoni, P.M., Unsworth, M.H., Law, B.E., Irvine, J., Baldocchi, D.D., Van Tuyl, S., Moore, D., 2002. Seasonal differences in carbon and water vapor exchange in young and old-growth ponderosa pine ecosystems. Agric. Forest Meteorol. 111, 203–222.

Aubinet, M., Heinesch, B., Yernaux, M., 2003. Horizontal and vertical CO_2 advection in a sloping forest. Boundary Layer Meteorol. 108 (3), 397–417.

Benner, R.L., Lamb, B., 1985. A fast response continuous analyzer for halogenated atmospheric tracers. J. Atmos. Oceanic Technol. 2, 582–589.

Black, T.A., Hartog, G.d., Neumann, H.H., Blanken, P.D., Yang, P.C., Russell, C., Nesic, Z., Lee, X., Chen, S.G., Staebler, R., Novak, M.D., 1996. Annual cycles of water vapour and carbon dioxide fluxes in and above a boreal aspen forest. Global Change Biol. 2, 219–229.

Bowling, D.R., Burns, S.P., Conway, T.J., Monson, R.K., White, J.W.C., 2005. Extensive observations of CO_2 carbon isotope content in and above a high-elevation subalpine forest. Global Biogeochem. Cycles 19.

Bowling, D.R., McDowell, N.G., Bond, B.J., Law, B.E., Ehleringer, J.A., 2002. [^{13}C] content of ecosystem respiration is linked to precipitation and vapor pressure deficit. Oecologia 131, 113–124.

Buchmann, N., Kao, W.-Y., Ehleringer, J.R., 1997. Influence of stand structure on carbon-13 of vegetation, soils, and canopy air within deciduous and evergreen forests in Utah, United States. Oecologia 110, 109–119.

Campbell, J.L., Law, B.E., 2005. Forest soil respiration across three climatically distinct chronosequences in Oregon. Biogeochemistry 73, 109–125.

Carlson, M.A., Stull, R.B., 1986. Subsidence in the nocturnal boundary layer. J. Climate Appl. Meteorol. 25, 1088–1099.

Clements, C.B., Whiteman, C.D., Horel, J.D., 2003. Cold-air-pool structure and evolution in a mountain basin: Peter Sinks, Utah. J. Appl. Meteorol. 42, 752–768.

Dobosy, R.J., Rao, K.S., Przybylowicz, J.W., Eckman, R.M., Hosker Jr., R.P., 1989. Mass and momentum balance in the Brush Creek drainage flow determined from single-profile data. J. Appl. Meteorol. 28, 467–476.

Doran, J.C., Horst, T.W., Whiteman, C.D., 1990. The development and structure of nocturnal slope winds in a simple valley. Boundary Layer Meteorol. 52, 41–68.

Ekblad, A., Högberg, P., 2001. Natural abundance of ^{13}C in CO_2 respired from forest soils reveals speed of link between tree photosynthesis and root respiration. Oecologia 127, 305–308.

Farquhar, G.D., Ehleringer, J.R., Hubick, K.T., 1989. Carbon isotope discrimination and photosynthesis. Ann. Rev. Plant Physiol. Plant Mol. Biol. 40, 503–537.

Finnigan, J., 2006. The storage term in eddy flux calculations. Agric. Forest Meteorol. 136, 108–113.

Finnigan, J.J., Clement, R., Mahli, Y., Leuning, R., Cleugh, H.A., 2003. A re-evaluation of long-term flux measurement techniques. Part 1: Averaging and coordinate rotation. Boundary Layer Meteorol. 107, 1–48.

Flaherty, J.F., Lamb, B., Allwine, K.J., Allwine, E. Vertical tracer concentration profiles measured during the Joint Urban 2003 Dispersion Study. J. Appl. Meteorol., in press.

Flanagan, L.B., Brooks, J.R., Varney, G.T., Berry, S.C., Ehleringer, J.A., 1996. Carbon isotope discrimination during photosynthesis and the isotope ratio of respired CO_2 in boreal forest ecosystems. Global Biogeochem. Cycles 10, 629–640.

Fleagle, R.G., 1950. A theory of air drainage. J. Meteorol. 7, 227–232.

Fons, W.L., 1940. Influence of forest cover on wind velocity. J. Forestry 38, 481–486.

Harmon, M.E., Bible, K., Ryan, M.G., Shaw, D.C., Chen, H., Klopatek, J., Li, X., 2004. Production, respiration, and overall carbon

balance in an old-growth *Pseudotsuga-Tsuga* forest ecosystem. Ecosystems 7, 498–512.

Hawkes, H.B., 1947. Mountain and Valley Winds with Special Reference to the Diurnal Mountain Winds of the Great Salt Lake Region. Ohio State University, Columbus, p. 312.

Högberg, P., Nordgren, A., Buchmann, N., Taylor, A.F.S., Ekblad, A., Högberg, M.N., Nyberg, G., Ottosson, Löfvenius, M., Read, D.J., 2001. Large-scale forest girdling shows that current photosynthesis drives soil respiration. Nature 411, 307–789.

Iijima, Y., Shinoda, M., 2000. Seasonal changes in the cold-air pool formation in a subalpine hollow, central Japan. Int. J. Climatol. 20, 1471–1483.

Jiabing, W., Dexin, G., Miao, W., Tiefan, P., Shijie, H., Changjie, J., 2006. Year-round soil and ecosystem respirtion in a temperate broad-leaved Korean pine forest. Forest Ecol. Manage. 223, 35–44.

Keeling, C.D., 1958. The concentration and isotopic abundances of atmospheric carbon dioxide in rural areas. Geochim. Cosmochim. Acta 13, 322–334.

Keeling, C.D., 1961. The concentration and isotopic abundances of carbon dioxide in rural and marine air. Geochim. Cosmochim. Acta 24, 277–298.

King, C.W., 1989. Representativeness of single vertical wind profiles for determining volume flux in valleys. J. Appl. Meteorol. 28, 463–466.

Lamb, B.K., McManus, J.B., Shorter, J.H., Kolb, C.E., Mosher, B., Harriss, R.C., Allwine, E., Blaha, D., Howard, T., Guenther, A., Lott, R.A., Siverson, R., Westberg, H., Zimmerman, P., 1995. Development of atmospheric tracer methods to measure methane emissions from natural gas facilities and urban areas. Environ. Sci. Technol. 29 (6), 1468–1479.

Landsberg, J.J.J.G.B., 1971. Wind profiles in plant canopies: studies on an analytical model. J. Appl. Ecol. 8 (3), 729–741.

Lavigne, M.B., Anderson, D.E., Ryan, M.G., Anderson, D.E., Baldocchi, D.D., Crill, P.M., Fitzjarrald, D.R., Goulden, M.L., Gower, S.T., Massheder, J.M., McCaughey, J.H., Rayment, M., Striegl, R.G., 1997. Comparing nocturnal eddy covariance measurements to estimates of ecosystem respiration made by scaling chamber measurements at six coniferous boreal sites. J. Geophys. Res. 105 (D24), 28977–28985.

Law, B.E., Thornton, P.E., Irvine, J., Anthoni, P.M., Van Tuyl, S., 2001. Carbon storage and fluxes in ponderosa pine forests at different developmental stages. Global Change Biol. 7, 755–777.

Magono, C., Nakamura, C., Yoshida, Y., 1982. Nocturnal cooling of the Moshiri Basin, Hokkaido in midwinter. J. Meteorol. Soc. Jpn. 60 (5), 1106–1116.

Mahrt, L., 1981. The early evening boundary layer transition. Quart. J. R. Meteorol. Soc. 107, 329–343.

Mahrt, L., 1986. Nocturnal Topoclimatology Ed. W.C. program. World Meteorological Organization, Geneva, p. 76.

Mahrt, L., Larsen, S., 1982. Small scale drainage front. Tellus 34, 579–587.

Maki, M., Harimaya, T., 1988. The effect of advection and accumulation of downslope cold air on nocturnal cooling in basins. J. Meteorol. Soc. Jpn. 66, 581–597.

Manins, P.C., Sawford, B.L., 1979. Katabatic winds: a field study. Quart. J. Meteorol. Soc. 105, 1011–1025.

Moore, G.W., Bond, B.J., Jones, J.A., Phillips, N., Meinzer, F.C., 2004. Structural and compositional controls on transpiration in a 40- and 450-yr-old riparian forest in western Oregon, USA. Tree Physiol. 24, 481–491.

Mori, M., Kobayashi, T., 1996. Dynamic interaction between observed nocturnal drainage winds and a cold air lake. J. Meteorol. Soc. Jpn. 74 (2), 247–258.

Neff, W.D., King, C.W., 1989. The accumulation and pooling of drainage flows in a large basin. J. Appl. Meteorol. 28, 518–529.

Nikus, U., Vergeiner, I., 1984. The thermal structure of the Inn Valley atmosphere. Arch. Meteorol. Geophys. Bioclimatol. A33, 199–215.

Parsons, E.A., Mote, P.W., Hamlet, A., Mantua, N., Snover, A., Keeton, W., Miles, E., Canning, D., Gray Ideker, K., 2001. Potential consequences of climate variability and change for the Pacific Northwest. In: Team, N.A.S. (Ed.), Climate Change Impacts of the United States: The Potential Consequences of Climate Variability and Change: Foundation Report. Cambridge University Press, New York, pp. 247–280.

Paw U, K.T., Falk, M., Suchanek, T.H., Ustin, S.L., Chen, J., Park, Y.-S., Winner, W.E., Thomas, S.C., Hsiao, T.C., Shaw, R.H., King, T.S., Pyles, R.D., Schroeder, M., Matista, A.A., 2004. Carbon dioxide exchange between an old-growth forest and the atmosphere. Ecosystems 7, 513–524.

Pypker, T.G., Mix, A.C., Unsworth, M.H., Rugh, W., Ocheltree, T., Alstad, K., Bond, B.J., 2007. Using nocturnal cold air drainage flow to monitor ecosystem processes in complex terrain: a pilot study on the carbon isotopic composition, advection of ecosystem, respiration. Ecol. Appl. 17, 702–714.

Schimel, D.S., Kittel, T.G.F., Running, S.W., Monson, R.K., Turnipseed, A.A., Anderson, D.E., 2002. Carbon sequestration studies in Western US mountains. EOS 83, 445–448.

Shaw, R.H., 1977. Secondary wind speed maxima inside plant canopies. J. Appl. Meteorol. 16, 514–521.

Soler, M.R., Infante, C., Buenestado, P., Mahrt, L., 2002. Observations of nocturnal drainage flow in a shallow gully. Boundary-Layer Meteorol. 105, 253–273.

Staebler, R.M., Fitzjarrald, D.R., 2004. Observing subcanopy CO_2 advection. Agric. Forest Meteorol. 122, 139–156.

Stull, R.B., 1988. An Introduction to Boundary Layer Meteorology. Kluwer Academic Publishers, Boston, p. 666.

Swanson, F.J., James, M.E., 1975. Geology and geomorphology of the H.J. Andrews Experimental Forest, Western cascades, Oregon. Pacific Northwest Forest and Range Experiment Station, Forest Service, U.S.D.A, Research Paper PNW-188, pp. 1–14.

Taylor, G.H., Hannan, C., 1999. The Climate of Oregon: From Rainforest to Desert. Oregon State University Press, Corvallis, p. 211.

Turnipseed, A.A., Anderson, D.E., Blanken, P.D., Baugh, W.M., Monson, R.K., 2003. Airflows and turbulent flux measurements in mountainous terrain: part 1. Canopy and local effects. Agric. Forest Meteorol. 119, 1–21.

Valentini, R., Dore, S., Marchi, G., Mollicone, D., Panfyorov, M., Rebmann, C., Kolle, O., Schulze, E.-D., 2000. Carbon and water exchanges of two contrasting central Siberia landscape types: regenerating forest and bog. Funct. Ecol. 14, 87–96.

Whiteman, C.D., 1982. Breakup of temperature inversions in deep mountain valleys: part I. Observations. J. Appl. Meteorol. 21, 270–289.

Whiteman, C.D., 1986. Temperature inversion buildup in Colorado's Eagle Valley. Meteorol. Atmos. Phys. 35, 220–226.

Whiteman, C.D., 1990. Observations of thermally developed wind systems in mountainous terrain. In: Blumen, W (Ed.), Atmospheric Processes Over Complex Terrain. American Meteorological Society, Boston, pp. 5–42.

Whiteman, C.D., Allwine, K.J., Fritschen, L.J., Orgill, M.M., Simpson, J.R., 1989. Deep valley radiation and surface energy budget microclimates. Part II: Energy budget. J. Appl. Meteorol. 28, 427–437.

Whiteman, C.D., Pospichal, B., Eisenbach, S., Weihs, P., Clements, C.B., Steinacker, R., Mursch-Radlgruber, E., Dorninger, M., 2004. Inversion breakup in small rocky mountain alpine basins. J. Appl. Meteorol. 43, 1069–1082.

Yi, C., Monson, R., Zhai, Z., Anderson, D.E., Lamb, B., Allwine, G., Turnipseed, A.A., Burns, S.P., 2005. Modeling and measuring the nocturnal drainage flow in high-elevation, subalpine forest with complex terrain. J. Geophys. Res., 110, p. D22303, doi:10.1029/2005JD006282.

Yoshino, M.M., 1984. Thermal belt and cold air drainage on the mountain slope and cold air lake in the basin at quiet, clear night. GeoJournal 8 (3), 235–250.